8434 *Biochemistry* **2010,** *49,* 8434–8441
DOI: 10.1021/bi1007595

BIOCHEMISTRY
including biophysical chemistry & molecular biology
Article

Comparative Kinetics of Cofactor Association and Dissociation for the Human and Trypanosomal *S*-Adenosylhomocysteine Hydrolases. 3. Role of Lysyl and Tyrosyl Residues of the C-Terminal Extension[†]

Sumin Cai,[‡] Jianwen Fang,*[,⊥] Qing-Shan Li,[§] Ronald T. Borchardt,[§] Krzysztof Kuczera,[‡,∥] C. Russell Middaugh,[§] and Richard L. Schowen[‡,§,∥]

[‡]*Department of Molecular Biosciences,* [§]*Department of Pharmaceutical Chemistry,* [∥]*Department of Chemistry, and* [⊥]*Applied Bioinformatics Laboratory, The University of Kansas, Lawrence, Kansas 66047*

Received May 12, 2010; Revised Manuscript Received August 3, 2010

ABSTRACT: On the basis of the available X-ray structures of *S*-adenosylhomocysteine hydrolases (SAHHs), free energy simulations employing the MM-GBSA approach were applied to predict residues important to the differential cofactor binding properties of human and trypanosomal SAHHs (Hs-SAHH and Tc-SAHH), within 5 Å of the cofactor NAD^+/NADH binding site. Among the 38 residues in this region, only four are different between the two enzymes. Surprisingly, the four nonidentical residues make no major contribution to differential cofactor binding between Hs-SAHH and Tc-SAHH. On the other hand, four pairs of identical residues are shown by free energy simulations to differentiate cofactor binding between Hs-SAHH and Tc-SAHH. Experimental mutagenesis was performed to test these predictions for a lysine residue and a tyrosine residue of the C-terminal extension that penetrates a partner subunit to form part of the cofactor binding site. The K431A mutant of Tc-SAHH (TcK431A) loses its cofactor binding affinity but retains the wild type's tetrameric structure, while the corresponding mutant of Hs-SAHH (HsK426A) loses both cofactor affinity and tetrameric structure [Ault-Riche, D. B., et al. (1994) *J. Biol. Chem. 269*, 31472−31478]. The tyrosine mutants HsY430A and TcY435A alter the NAD^+ association and dissociation kinetics, with HsY430A increasing the cofactor equilibrium dissociation constant from approximately 10 nM (Hs-SAHH) to ∼800 nM and TcY435A increasing the cofactor equilibrium dissociation constant from approximately 100 nM (Tc-SAHH) to ∼1 mM. Both changes result from larger increases in the off rate combined with smaller decreases in the on rate. These investigations demonstrate that computational free energy decomposition may be used to guide experimental studies by suggesting sensitive sites for mutagenesis. Our finding that identical residues in two orthologous proteins may give significantly different binding free energy contributions strongly suggests that comparative studies of homologous proteins should investigate not only different residues but also identical residues in these proteins.

Mammals (*1*) and the protozoan parasites *Trypanosoma* (*2*), *Plasmodium* (*3*), and *Leishmania* (*4*) all have *S*-adenosyl-L-homocysteine hydrolases (SAHHs),[1] which catalyze the hydrolysis of *S*-adenosyl-L-homocysteine (AdoHcy) to adenosine (Ado) and L-homocysteine (Hcy). SAHHs are metabolically important enzymes because AdoHcy is a feedback inhibitor of *S*-adenosylmethionine (AdoMet)-dependent transmethylation enzymes that play crucial roles in regulating methylation of a variety of macromolecules and small molecules (*5*). For this reason, SAHHs have been considered as possible antiparasitic drug targets. The catalytic mechanism of SAHHs includes a complete redox cycle of a nicotinamide cofactor (NAD^+/NADH) that is tightly bound within the enzyme (*1*, *6*). The catalytic properties of human and parasitic SAHHs are very similar. This discourages the design of antiparasitic drugs as substrate analogues or mechanism-based inhibitors. Our studies of human SAHH (Hs-SAHH) and trypanosomal SAHH (Tc-SAHH), however, reveal significant differences in the kinetics and thermodynamics of nicotinamide cofactor binding between these two enzymes (*7*). This provides possible approaches to the design of inhibitors having differential effects on Tc-SAHH compared to Hs-SAHH. Such inhibitors may benefit patients who suffer from Chagas disease which is transmitted by the parasite *Trypanosoma cruzi* (*8*).

Several X-ray crystallographic structures of Hs-SAHH such as Protein Data Bank (PDB) entries 1A7A (*1*) and 1LI4 (*6*), and Tc-SAHH [PDB entry 1XBE (unpublished data of Q.-S. Li and W. Huang)] are available. Both SAHHs are homotetramers, and each subunit contains a substrate-binding domain, a cofactor (NAD^+/NADH)-binding domain, and a C-terminal tail that covers the cofactor-binding site of the neighboring subunit (Figure 1).

[†]This study was supported by Grant GM-29332 from the National Institute of General Medical Sciences.

*To whom correspondence should be addressed: Applied Bioinformatics Laboratory, 2034 Becker Dr., The University of Kansas, Lawrence, KS 66047. Telephone: (785) 864-3349. Fax: (785) 864-8141. E-mail: jwfang@ku.edu.

[1]Abbreviations: 2×YT, 2×x yeast extract tryptone; Ado, adenosine; AdoHcy, *S*-adenosyl-L-homocysteine; DTT, DL-dithiothreitol; EDTA, ethylenediaminetetraacetic acid; FPLC, fast protein liquid chromatography; Hcy, L-homocysteine; HPLC, high-performance liquid chromatography; Hs-SAHH, SAHH from *Homo sapiens* (human placenta); NAD^+, β-nicotinamide adenine dinucleotide; NADH, β-nicotinamide adenine dinucleotide, reduced form; SAHH, *S*-adenosyl-L-homocysteine hydrolase (EC 3.1.1.1); Tc-SAHH, SAHH from *Trypanosoma cruzi*; rmsd, root-mean-square deviation; MM-GBSA, Molecular Mechanics-Generalized Born Surface Area; DHCeA, (1′*R*,2′*S*,3′*R*)-9-(2′,3′-dihydroxycyclopent-4′-enyl)adenine; NepA, neplanocin A.

 Published on Web 08/05/2010

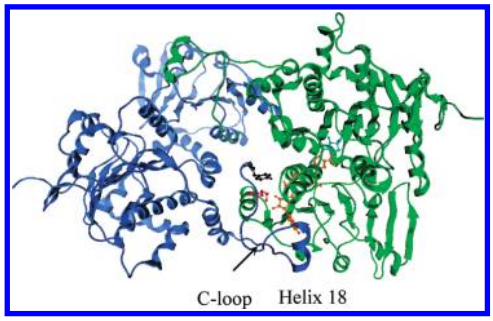

FIGURE 1: "Dimer" structure of SAHHs that forms a part of the overall tetrameric enzyme structure (*1*). The monomers are colored blue and green, with cofactor ligands in gold ball-and-stick representations and a substrate analogue ligand in a turquoise ball-and-stick representation. The C-terminal extension of each monomer, containing helix 18, can be seen penetrating into the partner monomer to form part of the cofactor-binding site (top left, green; bottom right, blue). K426 (in red ball-and-stick representation) and Y430 (in black ball-and-stick representation) (Hs-SAHH) are located in the final coil between helix 18 and the C-terminus.

A lysine and a tyrosine located within the C-terminal chain are very close to the NAD(H) cofactor in the X-ray structures and may provide important contributions to cofactor binding of SAHHs. Two main conformations of SAHH have been characterized: a ligand-free "open" form with the cofactor NAD^+ bound (*9*) and a "closed" form containing the cofactor NADH and oxidized substrate [DHCeA (*1*) or NepA (*6*)]. The atomic-level mechanism of the differential nicotinamide cofactor binding properties of Hs-SAHH and Tc-SAHH, however, is not yet clear (*7*).

To analyze microscopic differences between NAD binding to Hs-SAHH and Tc-SAHH, we have estimated cofactor binding free energy decompositions based on the MM-GBSA approach (*10*). The free energy decomposition estimations permit the prediction of residues that significantly contribute the most to cofactor binding. In this study, experimental mutagenesis was then performed to test computational predictions for two pairs of conserved residues: a lysine and a tyrosine in the C-terminal tail in both enzymes. For a majority of these mutants, the experimental results were qualitatively consistent with the computational predictions, confirming the utility of MM-GBSA free energy estimations for identification of functionally important protein sites.

MATERIALS AND METHODS

Computational Procedures. The starting crystallographic structures of Hs-SAHH and Tc-SAHH were downloaded from the PDB (entries 1A7A and 1XBE, respectively). Calculations for another crystal structure of Hs-SAHH (PDB entry 1IL4) yielded very similar results. Thus, only the data for the 1A7A structure are shown in this study. The 1A7A structure was originally determined by incorporation of selenium atoms (SE) in place of the sulfurs in Met residues. Assuming that this does not influence structure, we replaced Se atoms with S atoms and renamed the residues (from MSE to MET). The simulation system was set up using the Xleap module of Amber 7 (http://ambermd.org/). The SAHH homotetramer is a "dimer of dimers", with one of the dimers formed by subunits A and B and the other formed by subunits C and D. In brief, the protein (the AB dimer, each subunit bound with one NADH and one inhibitor) was solvated using a periodic truncated octahedral box of 29419 water molecules, as described by the TIP3P model (*11*), and extended to a distance of 10 Å from any solute atom. The system was then neutralized by 16 sodium cations initially placed around the protein using a Coulombic potential on a grid. All minimization and molecular dynamics (MD) were performed with the Amber 7 suite of programs. The ff99 force field was used for proteins and NADH cofactor throughout the energy minimization and MD simulations. The starting geometry of ligands was taken from the protein PDB files. The input files for ligand MD simulations were prepared with the antechAmber program in Amber 7, which uses the General Amber Force Field (GAFF). Partial charges on the ligand atoms were calculated with the AM1-BCC method available in antechAmber (*12*).

(*i*) *Energy Minimization*. The energy minimization was performed using the sander module in the Amber 7 suite of programs with the particle-mesh Ewald method for inclusion of long-range electrostatic interactions (*13*). We used two stages of energy minimization. In the first stage, only water molecules were minimized while the protein was fixed. The second stage minimized the entire system. Each stage was conducted with 500 cycles of steepest descent followed by 4500 conjugate steps of gradient minimization. The nonbonded cutoff was set to 12.0 Å.

(*ii*) *Molecular Dynamics Simulations*. The equilibration process was conducted in two stages following the protocol suggested in the Amber 7 manual. In the first stage, the system was heated gradually from a low temperature of 100 to 300 K over a 10 ps simulation time with a time step of 2 fs. A cutoff distance of 12 Å was used for the nonbonded interaction. The SHAKE algorithm was used to constrain the bonds involving hydrogen atoms, and the force evaluations for these bonds were omitted (*14*). A periodic boundary with a constant volume and without pressure control was used. Then a second 10 ps equilibration was continued under a constant pressure and a constant temperature with isotropic position scaling to adjust the density of water to experimental values. After that, the entire system was equilibrated for 100 ps at a constant temperature of 300 K and a constant pressure of 1 bar. The SHAKE algorithm and 2 fs time steps were employed throughout all MD stages.

A 500 ps production run was performed with the same protocol used in the final stage of equilibration. After the simulation was completed, the ptraj module in Amber 7 was used to reimage the whole trajectory (including all equilibration and production runs), to remove the waters and Na^+ from the trajectory file, and to calculate the root-mean-square deviations (rmsd) of backbone atoms from the starting structure over the entire course. Fifty snapshots were taken at 2 ps intervals from the section of the MD trajectory where the rmsd reached a plateau and were used for further analysis. These sections corresponded to an rmsd of ~1.5 Å for Hs-SAHH and an rmsd of ~1.3 Å for Tc-SAHH.

(*iii*) *Calculation of Energy Decomposition by MM-GBSA*. The residue-level free energy contributions to the cofactor binding were estimated using the MM-GBPA approach implemented in the mm_pbsa.pl script available in the Amber package. MM-GBSA is a postprocessing method that can be used to evaluate free energy contributions at the residue level of binding of molecules in solution (*15*). It combines the molecular mechanical energies with the implicit solvent approaches. The molecular mechanical energies, representing internal energy, van der Waals, and electrostatic interactions, are calculated using the sander program in Amber. The generalized Born (GB) model implemented in sander is used to estimate the electrostatic contribution to the solvation free energy, and the solvent-accessible surface area-dependent term is used to determine the

hydrophobic contribution to the solvation energy. The conformational entropies could be estimated using normal-mode analysis but were not considered because of computer resource limitations. The entropic term is probably much smaller than the others and may be neglected in comparative studies of very similar systems (*10*). In this study, we used the single-trajectory protocol (*10*) based on the assumption that the snapshots of the protein and cofactor taken from the complex trajectory are similar to those that would emerge from separate trajectories of the protein and cofactor, or that the differences in the snapshots of single and separate trajectories are consistent between Hs-SAHH and Tc-SAHH. Both circumstances are considered acceptable because we were interested in the relative difference of the free energy contributions in these residues in Tc-SAHH and Hs-SAHH.

The simulated complex was a dimer bound with two cofactors and inhibitors [closed-form Hs-SAHH with DHCeA (PDB entry 1A7A) and closed-form Tc-SAHH with NepA (PDB entry 1XBE)]. In the analysis of individual residue contributions to ΔG, we considered only the 38 residues within 5 Å of the NAD(H) binding site in Hs-SAHH as well as Tc-SAHH. We calculated the difference of free energy contributions of all of these residues.

Experimental Procedures. (*i*) *Construction of the Mutants of Hs-SAHH and Tc-SAHH*. The wild-type genes of Hs-SAHH and Tc-SAHH were each inserted into their own copy of the pPROK-1 vector (Clontech). Three alanine mutants (HsY430A, TcK431A, and TcY435A) were prepared by the site-directed mutagenesis PCR. The following primer sequences were used: HsY430A, 5′-CAAGCCGGATCACGCCCGCTACTGAGA-3′ and 5′-TCTCAGTAGCGGGCGTGATCCGGCTTG-3′; TcK431A, 5′-ACGGCCCATTCGCGCCGGACCACTACC-3′ and 5′-GGTAGTGGTCCGGCGCGAATGGGCCGT-3′; TcY435A, 5′-AAGCCGGACCACGCCCGCTACTAATCG-3′ and 5′-CGATTAGTAGCGGGCGTGGTCCGGCTT-3′.

The amplification reactions of HsY430A, TcK431A, and TcY435A were performed in a volume of 50 μL containing 20 ng of template, 25 pmol of 5′ and 3′ primers, 12.5 nmol of each deoxynucleoside triphosphate, 3 units of native Pfu DNA polymerase (Stratagene), 6 μL of 10× Pfu buffer, and 2.5 μL of DMSO. The steps of the PCR program were set up as follows: (1) 92 °C for 4 min, (2) 25 cycles of 92 °C for 30 s, 52 °C for 30 s, and 68 °C for 20 min, (3) 68 °C for 10 min, and (4) hold at 4 °C. The PCR products of HsY430A and TcK431A were purified with a Qiagen PCR purification kit, while the PCR product of TcY435A contains two fragments of different sizes. The correct size band (large size) was cut and collected from a 1% DNA gel (low melting point), and then the PCR product was recycled with a Qiagen gel extraction kit. These three purified PCR products were digested with DpnI (Biolab) and transformed into *Escherichia coli* competent cell strain JM109 (Sigma). The purified mutant genes were confirmed by DNA sequencing.

(*ii*) *Purification of the Mutants of Hs-SAHH and Tc-SAHH*. The procedures for overexpression (*7*), purification (*7*), and cell-free extract preparation (*16*) of the Hs-SAHH and Tc-SAHH mutants were similar to those previously described for the wild-type SAHHs with modifications as follows. The cell-free extracts were passed through a FPLC system (Amersham Biosciences), including four different columns, namely, a Q-Sepharose Fast Flow column (26/10), a Hiload Phenyl-Sepharose column (26/10), a Hiload Superdex 200 column (16/60), and MonoQ column (10/10). Buffer A consisted of 25 mM Tris-HCl buffer (pH 7.4), 1 mM EDTA, and 40 μM NAD^+. Buffer B consisted of 80 mM Tris-HCl buffer (pH 7.4), 1 mM EDTA, 1 M NaCl, and 40 μM NAD^+. After the Q-Sepharose Fast Flow column (26/10), mutant proteins were identified by SDS−PAGE. The mutant TcK431A was purified employing only Q-Sepharose Fast Flow (26/10) and Hiload Superdex 200 (16/60) columns.

(*iii*) *Hydrolytic Activity Assay*. The procedures for measuring SAHH activity in the hydrolytic direction were as described previously (*16*). The generated Ado was quickly removed by Ado deaminase to drive completion of the hydrolytic reaction. The rate of Hcy production was coupled with the formation of TNB^{2-} from DTNB. TNB^{2-} is intensely yellow and was identified at the absorption wavelength of 412 nm by UV spectroscopy.

(*iv*) *Reconstitution of the NAD^+ Form and NADH Form of Hs-SAHH and Tc-SAHH Mutants*. Preparation of the apo forms of Hs-SAHH and Tc-SAHH mutants and reconstitution of the NAD^+ and NADH forms of Hs-SAHH and Tc-SAHH mutants followed the same procedures described previously for wild-type SAHHs (*16*). Apo forms of SAHH mutants were prepared by using 80% (v/v) acid ammonium sulfate with 2−5 mM DTT to precipitate purified mutants three times (pH 2.92, 3.12, and 7.2). The proteins collected by centrifugation were dissolved in 50 mM phosphate buffer (pH 7.2) containing 1 mM EDTA. NAD^+ (1 mM) or NADH (1 mM) was incubated with 10 mg/mL apo forms of the SAHH mutants for 12 h at 4 °C. The reconstituted NAD^+ (or NADH) form of the mutants was then purified with a Hiload Superdex 200 column (16/60) (Amersham Sciences).

(*v*) *Determination of the Contents of NADH in the Isolated Hs-SAHH and Tc-SAHH Mutants*. The mutant proteins [395 μg in 90 μL of 50 mM phosphate buffer (pH 7.2) and 1 mM EDTA] were mixed with 10 μL of 1 M Na_2CO_3/$NaHCO_3$ (pH 10.7). A volume of 700 μL of 95% ethanol was then added to denature proteins and release NADH into solution. After centrifugation at 13400 rpm for 10 min to remove precipitated proteins, the fluorescence intensity of NADH was measured by a photon technologies QM-3 scanning luminescence spectrophotometer. The excitation wavelength was 340 nm, and the emission wavelength was 450 nm. NADH standards were prepared at concentrations ranging from 0.1 to 10 μM and were used to determine NADH content. The NADH content of SAHH inactivated by NepA was used as a control (100% NAD^+ reduced to NADH).

(*vi*) *Determination of the Contents of NAD^+ in Hs-SAHH and Tc-SAHH Mutants*. The mutant proteins [395 μg in 80 μL of 50 mM KPB (pH 7.2) and 1 mM EDTA] were denatured by addition of 2 μL of 5 M $HClO_4$. Samples were centrifuged at 13400 rpm for 10 min at 4 °C to remove precipitated proteins. The supernatant was injected into a reversed-phase C18 column (Vydac 218TP54, 300 Å, 5 μm, 4.5 mm × 250 mm) to measure the concentration of NAD^+ at 258 nm. The NAD^+ standard curve was made for the range of 1−200 μM. NAD^+ was eluted from the HPLC column at ~5.9 min by a gradient of 2 to 10% mobile phase B over 20 min with a flow rate of 1 mL/min. Mobile phase A contained 10 mM 1-heptanesulfatic acid and 50 mM sodium phosphate (pH 3.2), while mobile phase B contained 80% acetonitrile and 20% 2-propanol.

RESULTS

Computational Results. (*i*) *Single-Residue Contributions to the Free Energy of NADH Binding to Hs-SAHH*

Table 1: Contributions to the Cofactor Binding Free Energies of the 38 Residues within 5 Å of the NAD(H) Binding Site in Hs-SAHH and Tc-SAHH in Units of Kilocalories per Mole[a]

Hs-SAHH residue	Thr157	Thr158	Thr159	Asn181	Lys186	Asp190	*Asn191*	Cys195	**Ala219**	Gly220
free energy contribution	−2.16	−6.26	−1.48	0.04	−0.72	0.1	*−6.29*	−0.6	**−0.9**	−1.55
Tc-SAHH residue	Thr156	Thr157	Thr158	Asn180	Lys185	Asp189	*Asn190*	Cys194	**Cys218**	Gly219
free energy contribution	−3	−6.88	−1.54	−0.29	−1.36	0.45	*−1.55*	−0.16	**−0.86**	−1.3
Hs-SAHH residue	Tyr221	Gly222	Asp223	Val224	Gly225	Thr242	*Glu243*	**Ile244**	Asp245	Asn248
free energy contribution	−1.44	−5.23	−0.36	−5.19	−0.51	−0.15	*−3.3*	**−3.06**	0.27	−1.19
Tc-SAHH residue	Tyr220	Gly221	Asp222	Val223	Gly224	Thr241	*Glu242*	**Val243**	Asp244	Asn247
Free energy Contribution	−0.79	−3.61	0	−4.71	−0.12	−0.23	*−9.68*	**−2.42**	0.16	−0.11
Hs-SAHH residue	Thr275	Thr276	Gly277	**Cys278**	Ile281	Ile299	Gly300	His301	Glu305	Leu344
free energy contribution	−0.26	−3.18	−0.27	**−0.34**	−1.23	−1.63	−1.41	−0.13	0.34	−0.6
Tc-SAHH residue	Thr274	Thr275	Gly276	**Asn277**	Ile280	Ile298	Gly299	His300	Glu304	Leu343
fee energy contribution	−0.13	−3.56	−0.96	**−0.67**	−0.98	−1.85	−1.09	−1.96	0.5	−0.52
Hs-SAHH residue	Asn346	His353	Thr407[b]	Leu409[b]	Gln413[b]	**Leu417**[b]	*Lys426*[b]	*Tyr430*[b]		
free energy contribution	−2.84	−0.46	−0.99	−0.63	0.02	**−0.17**	*−10.01*	*−3.87*		
Tc-SAHH residue	344 Asn	352 His	Thr412[b]	Leu414[b]	Gln418[b]	**Ile422**[b]	*Lys431*[b]	*Tyr435*[b]		
free energy contribution	−2.08	0.06	−0.58	−0.19	0.12	**−1.06**	*−2.65*	*−0.49*		

[a]Four pairs of nonidentical residues are shown in bold, while four pairs of residues are shown in italics due to the significant difference in their free energy contribution. [b]These residues are from the tail of the second chain.

and Tc-SAHH. Hs-SAHH and Tc-SAHH share ~70% of their amino acid sequences. In superimposed structures of Hs-SAHH and Tc-SAHH, with the superposition centered on the center of mass of the cofactor NADH, there are 38 protein residues within a 5 Å thick shell around the cofactor. To identify protein residues with the largest contributions to differential cofactor binding of Hs-SAHH and Tc-SAHH, contributions to the NADH binding free energy from every residue within 5 Å of the cofactor binding site were calculated, and the results are listed in Table 1. Thirty-four of these 38 residues (89%) are identical in Hs-SAHH and Tc-SAHH, while four pairs are different. In most cases, the individual residue contributions to cofactor binding are very similar in the two proteins. Interestingly, four pairs of identical residues (HsAaaTc: 191Asn193, 243Glu242, 426Lys431, and 430Tyr435), which are in italics in Table 1, make significantly different free energy contributions to the binding of NADH to Hs-SAHH and Tc-SAHH.

Experimental Results. (*i*) *Y430 in the C-Terminal Extension of Hs-SAHH May Slightly Influence Binding of NAD*$^+$ *and NADH to Apo-Hs-SAHH*. The mutant HsY430A is a purified protein of the correct molecular mass (190 kDa) and possesses an intact tetrameric structure (as evaluated by size exclusion chromatography). The enzyme is isolated from the expression system with 30 ± 5% active site occupancy by NAD$^+$ (HPLC) and 86 ± 5% active site occupancy by NADH (fluorescence). Denaturation of the isolated enzyme yielded 3.1 ± 0.1% adenosine and 81 ± 1% adenine. Reconstitution of apo-HsY430A with NAD$^+$ yielded a protein with 79 ± 1% occupancy (HPLC) and 70 ± 1% catalytic activity. Reconstitution of apo-HsY430A with NADH yielded a protein with 94 ± 1% occupancy (fluorescence).

(*ii*) *K431 in the C-Terminal Extension of Tc-SAHH Is Required for the Binding of NAD*$^+$ *and NADH to Apo-Tc-SAHH*. The purified mutant TcK431A was also of the correct molecular mass (194 kDa) and possesses an intact tetrameric structure (size exclusion chromatography). The enzyme is isolated from the expression system with no NAD$^+$ present (detection limit of 0.1% active site occupancy) and little NADH occupancy (1.30 ± 0.03% active site occupancy as determined by fluorescence). Attempts at reconstitution with the cofactor of apo-TcK431A yielded no detectable occupancy by either NAD$^+$ or NADH.

(*iii*) *Y435 in the C-Terminal Extension of Tc-SAHH Is Required for Tight Binding of NAD*$^+$ *and NADH to Apo-Tc-SAHH*. The mutant TcY435A was again of the correct molecular mass (194 kDa) and possesses an intact tetrameric structure (size exclusion chromatography). The enzyme is isolated from the expression system with 18 ± 1% active site occupancy by NAD$^+$ (HPLC) and 90 ± 1% active site occupancy by NADH (fluorescence). Denaturation of the isolated enzyme yielded 24 ± 1% adenosine and 65 ± 1% adenine. Attempted reconstitution of apo-TcY435A with NAD$^+$ or NADH yielded a protein with no detectable occupancy.

(*iv*) *Rate Constants for Dissociation of NAD*$^+$ *from Mutant SAHHs HsY430A and TcY435A Are 20- and 255-fold Larger, Respectively, Than Those for the Corresponding Wild-Type Enzymes*. The cofactor dissociated from the mutant enzymes in a simple first-order relaxation process [as previously observed in other cases (refs *7*, *9*, and *17* and unpublished data of Q.-S. Li) in which the enzymic activity proceeded from full activity to zero activity]. Mutant HsY430A released the cofactor at 30 °C and pH 7.4 with a k_{off} of (4.2 ± 0.1) × 10^{-4} s^{-1}, while the wild-type enzyme Hs-SAHH released the cofactor with a k_{off} of (1.9 ± 0.3) × 10^{-5} s^{-1}. The mutation therefore increases the dissociation rate constant by a factor of ~20. Mutant TcY435A released the cofactor at 24 °C and pH 7.4 with a k_{off} of (2.8 ± 0.2) × 10^{-2} s^{-1}, while the wild-type enzyme Tc-SAHH released the cofactor with a k_{off} of (1.1 ± 0.2) × 10^{-4} s^{-1}. The mutation therefore increases the dissociation rate constant by a factor of ~255. The values of these rate constants are included with other data in Table 2.

(*v*) *Association Kinetics of NAD*$^+$ *with Mutant SAHHs HsY430A and TcY435A*. These mutant enzymes exhibited (Supporting Information) association time courses like those seen with the other SAHHs (refs *7*, *9*, and *17* and unpublished data of Q.-S. Li): fast binding occurred within the dead time of the experiment, giving rise to an initial enzyme activity A_o; slow binding ensued with apparent first-order rate constant k_{app} and combined with A_o to give a final activity, A_f. Each of these three parameters is a function of NAD$^+$ concentration. The expected

Table 2: Values of Rate and Equilibrium Constants for the Kinetics of the Fast and Slow Binding Phases of the Association Reaction of NAD^+ with Hs-SAHH, HsY430A, Tc-SAHH, and TcY435A at 23 °C and pH 7.4, from References 7 and 17 and from Fits of the Data in Figure 2 to Equation 1a_1c

enzyme	K_o (μM), binding to fully functional sites of apo-SAHH	K_a (μM), binding to non functional sites of apo-SAHH	K_f (μM), binding to fully functional sites of holo-SAHH	$10^3 k_a$ (s^{-1}), transformation of nonfunctional apo sites to functional holo sites	$10^{-3} k_a/K_a$ (M^{-1} s^{-1}), binding and transformation of apo sites to holo sites	$10^{-3} k_{on}$ (M^{-1} s^{-1})	$10^6 k_{off}$ (s^{-1})	K_d (nM) [k_{off}/k_{on} or $k_{off}/(k_a/K_a)$]
Hs-SAHH	33 ± 4	19 ± 8	1.4 ± 0.3	55 ± 8	2.9 ± 1.2	1.9 ± 0.04	19 ± 3	10 ± 2
	n = 3.3 ± 1.4							7 ± 3
HsY430A	432 ± 93	17 ± 2	2.0 ± 0.3	9.5 ± 0.4	0.56 ± 0.07	0.54 ± 0.04	420 ± 10	784 ± 64
	n = 0.9 ± 0.1							750 ± 95
Tc-SAHH	38 ± 9	3.8 ± 0.6	1.8 ± 0.4	6.0 ± 0.2	1.6 ± 0.3	0.68 ± 0.02	110 ± 20	161 ± 30
	n = 1.6 ± 0.4							69 ± 18
enzyme	K_o (mM)	K_a (mM)	K_f (mM)	k_a (s^{-1})	k_a/K_a (M^{-1} s^{-1})	k_{on} (M^{-1} s^{-1})	$10^3 k_{off}$ (s^{-1})	K_d (mM)
TcY435A	2.6 ± 1	0.39 ± 0.04	0.20 ± 0.03	11 ± 0.4	29 ± 9	18 ± 2	28 ± 2	1.6 ± 0.2
	n = 0.6 ± 0.2							1.0 ± 0.3

dependencies on the basis of a model to be described in the Discussion are given by eqs 1a−1c.

$$A_o = (A_t/2)[[NAD^+]^n/(K_o{}^n + [NAD^+]^n)] \quad (1a)$$

$$A_f = A_t[[NAD^+]/(K_f + [NAD^+])] \quad (1b)$$

$$k_{app} = k_a[[NAD^+]/(K_a + [NAD^+])] \quad (1c)$$

where A_t is the total enzyme activity at saturating NAD^+ concentrations after completion of both phases of binding. Figure 2 shows (a) the dependencies on NAD^+ concentration of the fraction of fast binding A_o/A_t, the fraction of slow binding $(A_f - A_o)/A_t$, and the fraction of total binding A_f/A_t and (b) the dependence of k_{app} on NAD^+ concentration for the mutants HsY430A and TcY435A. The curves in Figure 2 represent least-squares best fits of eqs 1a−1c to the data, with parameters K_o, n, K_f, k_a, and K_a as given in Table 2.

DISCUSSION

Computed Free Energy Contributions of Individual Residues to the Cofactor Affinities of Hs-SAHH and Tc-SAHH Identify Four Conserved Residues as the Locus of Differential Cofactor Affinities. The 38 residues within 5 Å of the NAD(H) binding site that may form strong interactions with cofactor NAD(H) were chosen for this study. The structures of Hs-SAHH and Tc-SAHH were overlaid, and 34 of the 38 residue pairs were found to be identical. The four pairs of nonidentical residues were HsA219 and TcC218, HsI244 and TcV243, HsC278 and TcN277, and HsL417 and TcI422, shown in boldface in Table 1. None of these four nonidentical residues, however, makes a significant free energy contribution to the differential in the free energy of cofactor binding between Hs-SAHH and Tc-SAHH (Table 1). In fact, it is four pairs of identical residues [in italics in Table 1 (Hs/Tc: N191/N190, E243/E242, K426/K431, Y430/Y435)] that show the most significant differential free energy contributions (from ∼3.4 to ∼7.4 kcal/mol) to the cofactor binding of Hs-SAHH and Tc-SAHH.

In deciding which cases to address experimentally, we took note of the facts that Turner et al. (*18*) had identified HsK426 and HsY430 as of special interest because they are "involved in interactions with the NAD bound predominantly to the other monomer", an unusual feature of cofactor binding in SAHHs, and that Ault-Riché et al. (*19*) had prepared the mutant HsK426A and found it to be devoid of cofactor affinity and catalytic activity. We therefore decided to concentrate on HsK426, HsY430, and the corresponding residues of Ts-SAHH, TcK431 and TcY435.

Y430 in the C-Terminal Extension of Hs-SAHH Only Slightly Influences Binding of NAD^+ and NADH to Apo-Hs-SAHH. The mutant HsY430A continues to bind NAD^+ and NADH sufficiently strongly that the enzyme passes through the purification procedure from the expression system with essentially full occupancy of the cofactor sites (116 ± 7%). A preponderance of the cofactor sites was occupied by NADH (86 ± 5%). Denaturation resulted in the release of a small amount of adenine (∼3%) and a larger amount (81 ± 1%) of adenosine. One possible explanation for these observations is that at least part of the NADH arose by oxidation of adenosine in the active site to 3′-ketoadenosine, which can decompose to generate adenine, the fragments then remaining in the active site in the "closed" conformation (*1*, *6*) of the enzyme. The isolated enzyme could be converted to the apoenzyme and reconstituted to ∼79%

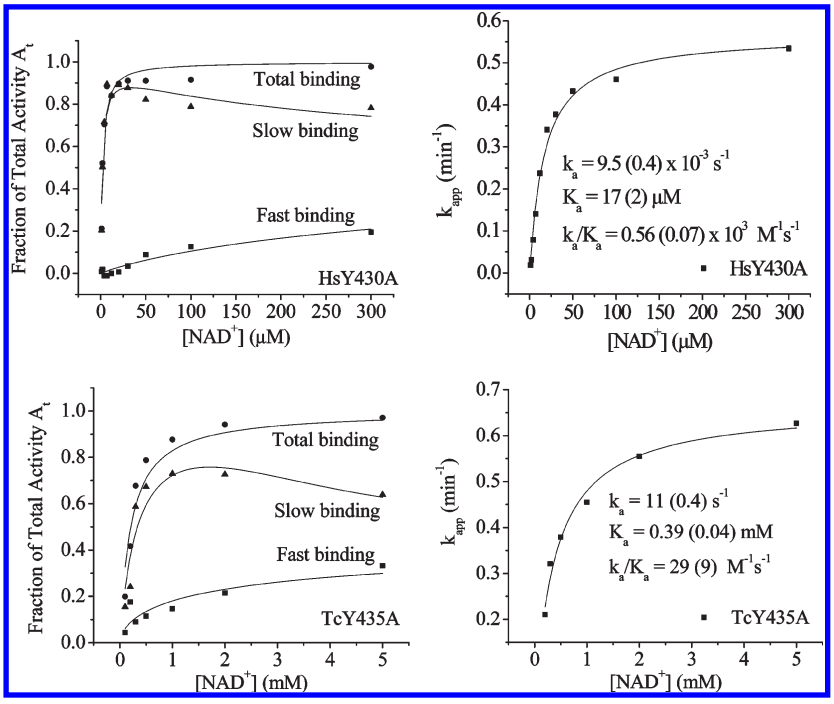

FIGURE 2: Fractions of fast binding, slow binding, and total binding of NAD^+ to the mutant enzyme HsY430A (left) and values of the slow binding rate constant k_{app} (right), both as a function of NAD^+ concentration (top panels). Fractions of fast binding, slow binding, and total binding of NAD^+ to the mutant enzyme TcY435A (left) and values of the slow binding rate constant k_{app} (right), both as a function of NAD^+ concentration (bottom panels). The curves are drawn from eqs 1a−1c with the least-squares best-fit parameters given in Table 2. Note that the concentration scales for HsY430A are below 300 μM while those for TcY435A go up to 5 mM.

occupancy by NAD^+, with the reconstituted enzyme exhibiting ~70% of the activity of the wild-type enzyme which has full occupancy of NAD^+. The HsY430A mutation thus has no large effect on the effective affinity of the enzyme for NAD^+ or NADH and little or no effect on the enzyme activity.

K431 in the C-Terminal Extension of Tc-SAHH Is Required for the Binding of NAD^+ and NADH to Apo-Tc-SAHH. The mutant TcK431A is the equivalent of the mutant HsK426A, prepared in previous work (*17*) and shown to have lost both cofactor affinity and tetrameric structure. TcK431A maintains its tetrameric structure but is isolated from the expression system without the cofactor and cannot be reconstituted under normal conditions with either NAD^+ or NADH. Thus, as with Hs-SAHH, this lysine residue is critical for the cofactor affinity (it is thought to form hydrogen bonds to the 2′- or 3′-OH group of the nicotinamide-bearing ribose ring) (*1*). It is striking that the mutation causes the loss of tetrameric structure in Hs-SAHH but not in Tc-SAHH. Previous comparisons (refs *7* and *17* and unpublished data of Q.-S. Li) of Hs-SAHH, Tc-SAHH, and their mutants have suggested that Hs-SAHH possesses a structure more robust with respect to mutation, typically showing smaller changes in its properties upon mutation than Tc-SAHH does. The quaternary structure would seem to be an exception to this rule.

Y435 in the C-Terminal Extension of Tc-SAHH Is Required for Tight Binding of NAD^+ and NADH to Apo-Tc-SAHH. The mutant TcY435A is the equivalent of HsY430A described above. Like HsY430A, the Tc mutant is isolated with high occupancy of the cofactor (mostly NADH) and releases a mixture of adenosine and adenine upon denaturation. Unlike HsY430A, the apo form of the Tc mutant no longer exhibits sufficient effective affinity for the cofactor to permit reconstitution. The kinetic experiments reported here were conducted with enzyme as isolated from the expression system.

Rate Constants for Dissociation of NAD^+ from Mutant SAHHs HsY430A and TcY435A Are 20- and 255-fold Larger, Respectively, Than Those for the Corresponding Wild-Type Enzymes. Experimental Results show that loss of the tyrosine in both enzymes increases the dissociation rate constant for NAD^+, but not for NADH. The increase is 1 order of magnitude larger for the human than for the Tc enzyme. This is consistent with the systematic observation cited above (refs *7*, *9*, and *17* and unpublished data of Q.-S. Li) that the human enzyme is less susceptible to mutational changes in its properties than the trypanosomal enzyme.

Association Kinetics of NAD^+ with Mutant SAHHs HsY430A and TcY435A. Cofactor combination with these mutant enzymes followed a model previously observed with Hs-SAHH, Tc-SAHH, and various mutants of both (refs *7*, *9*, *17* and unpublished data of Q.-S. Li). The elements of this model are as follows: (1) The apoenzyme possesses two equally numbered classes of active sites. (2) Half of the sites are capable of binding the cofactor rapidly (during the dead time of the experiment), with a relatively low affinity, and generating the full activity of these sites. This phenomenon accounts for the fast binding activity A_o observed at time zero from sites with cofactor dissociation constant K_o and Hill coefficient n. (3) Half of the apoenzyme sites (slow binding sites) are capable of binding the cofactor rapidly, with a relatively high affinity (dissociation constant K_a), but initially generating no enzymic activity. These events initiate a time-dependent reorganization with a rate constant k_a in which the slow binding sites acquire full enzymic activity and all sites acquire a common cofactor dissociation constant K_f, the final activity being A_f.

This model generates eqs 1a−1c, which were fit to the data as shown in Figure 2, producing the values of K_o, K_a, K_f, k_a, and n listed in Table 2. Table 2 also gives these values for Hs-SAHH and Tc-SAHH as determined previously (*7*). Finally, Table 2

presents values of the "on" rate constant for NAD^+, estimated as described in Materials and Methods by two different methods, and the "off" rate constant for NAD^+, obtained as described above. Together, these allow the calculation of the equilibrium constant K_d for NAD^+.

Comparison of the association kinetics for the wild-type enzymes Hs-SAHH and Tc-SAHH shows no dramatic differences. The value of k_{off} is ~5-fold larger for Tc-SAHH, and values of k_{on} are smaller by 2- or 3-fold; the result is a dissociation constant that is 10- or 20-fold larger.

The mutant HsY430A has lower affinity for the fast binding sites and a smaller reorganization rate constant k_a than Hs-SAHH, perhaps suggesting that some of the binding and reorganization events involve Y430 or its neighbors. The mutant off rate is > 20-fold larger and the on rate 4-fold lower than those for Hs-SAHH, resulting in a dissociation constant that is larger by ~100-fold.

The mutant TcY435A exhibits far more dramatic effects: the constants K_o, K_a, and K_f have all risen from the Tc-SAHH values of approximately micromolar values to around millimolar values, indicating that these affinities are significantly reduced by the removal of the tyrosine residue. The rate constant for reorganization is unaffected, but the off rate of the cofactor is increased by nearly 1000-fold; the on rates are smaller by ~100-fold. The result is cofactor binding with a millimolar dissociation constant in the mutant to a submicromolar dissociation constant for wild-type Tc-SAHH.

This relationship is similar to that for the HsY430A mutant and for the comparison of Tc-SAHH versus Hs-SAHH: a somewhat smaller decrease in on rate combines with a larger increase in off rate to generate weaker cofactor binding in the mutant enzyme compared to the wild-type enzyme or in Tc-SAHH compared to Hs-SAHH.

Why Do Identical Residues in Two Orthologous Proteins Make Significantly Different Contributions to the Binding Free Energy? In this study, the predicted differential contributions to the binding free energies of two pairs of identical amino acid residues have been largely confirmed by the experimental results, despite the intuitive notion that identical residues in two orthologous proteins should make similar binding free energy contributions. To investigate the reasons for this result, we examined the simulation snapshots of Tc-SAHH and Hs-SAHH. The C-loops of Hs-SAHH (red) and Tc-SAHH (blue) are superimposed and displayed, along with nearby NADHs, in Figure 3. We calculated the averages and standard errors of the distances from nitrogen atoms of Lys or oxygen atoms of Tyr to oxygen atoms of pyrophosphates between Tc-SAHH and Hs-SAHH. It is clear that these distances in Tc-SAHH and Hs-SAHH are different. Consequently, the strength of the hydrogen bonds formed between Tyr or Lys and NADH is significantly different in these two enzymes. We rationalize that the difference in distance between these C-loops and NADHs can be caused by the slightly different shape of the cofactor binding pocket or the overall conformation of the proteins, which originates from the sequence difference between these two proteins. Thus, "identical" residues in two nonidentical sequences should be regarded as only approximately identical.

CONCLUSION

Computational approaches and crystallographic structures of SAHHs suggest that a lysine residue and a tyrosine residue in a C-terminal extension of each subunit that forms part of the

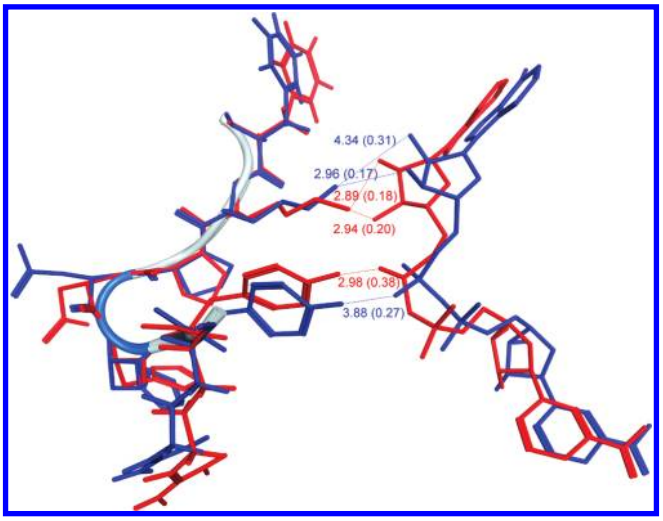

FIGURE 3: Superimposed C-loops of Hs-SAHH (red) and Tc-SAHH (blue) and nearby NADHs. The averages and standard errors of the distances from nitrogen atoms of Lys and oxygen atoms of Tyr to oxygen atoms of pyrophosphates are colored either red (for Tc-SAHH) or blue (for Hs-SAHH).

NAD^+/NADH binding site in a partner subunit might be critical for full cofactor affinity. Earlier work (*19*) showed that the K426A mutation of the human enzyme Hs-SAHH eliminated both cofactor affinity and the terameric structure of the enzyme. Here we show that the corresponding K431A mutation in the trypanosomal enzyme Tc-SAHH greatly reduces cofactor affinity but leaves the tetrameric structure intact, a rare example in which the trypanosomal enzyme appears more robust to mutational damage than the human enzyme. Residue HsY430 modulates the association−dissociation kinetics significantly in the case of Hs-SAHH, generating through its mutation to Ala a decreased cofactor affinity of just < 100-fold. The corresponding Y435A mutation in the Tc form decreased cofactor affinity by approximately 100000-fold. Both effects arise from a larger increase in the off rate of the cofactor, combined with a smaller decrease in the on rate. It should be noted that the values of K_f, the apparent dissociation constants of NAD^+ corresponding to a period immediately after mixing of apoenzymes with cofactor, are on the order of micromolar for both Hs-SAHH and Tc-SAHH (Table 2). Binding at this level persists or is strengthened by ~10-fold for Tc-SAHH but becomes stronger by ~100-fold for Hs-SAHH over a period of some hours, eventually reaching roughly nanomolar values of the dissociation constant [as reflected in the values of $k_{off}/(k_a/K_a)$ in Table 2]. This phenomenon was observed previously (*7*) but remains unexplained.

These investigations demonstrate that free energy decomposition may be used to guide experimental studies by suggesting sensitive sites for mutagenesis. Our finding that identical residues in two orthologous proteins may give significantly different binding free energy contributions strongly suggests that comparative studies of homologous proteins should investigate not only different residues but also identical residues in these proteins.

SUPPORTING INFORMATION AVAILABLE

Dependence of the concentrations of NAD^+ on the rate constants for the slow binding phase of the association of NAD^+ with the apo forms of mutant HsY430A and wild-type Hs-SAHHa at 23 °C and pH 7.4 (Figure S1), dependence of the concentrations of NAD^+ on the rate constants for the slow binding phase of the association of NAD^+ with the apo forms of mutant

TcY435A and wild-type Tc-SAHH (the wild-type Tc-SAHH data will be presented in detail elsewhere) at 23 °C and pH 7.4 (Figure S2), rmsd for the dynamic simulations of Hs-SAHH and Tc-SAHH (Figure S3), and rmsd for the predicted four identical residues that may give different binding free energy contributions in Hs-SAHH and Tc-SAHH (Figure S4). This material is available free of charge via the Internet at http://pubs.acs.org.

REFERENCES

1. Turner, M. A., Yang, X., Yin, D., Kuczera, K., Borchardt, R. T., and Howell, P. L. (2000) Structure and function of S-adenosylhomocysteine hydrolase. *Cell Biochem. Biophys. 33*, 101–125.
2. Parker, N. B., Yang, X., Hanke, J., Mason, K. A., Schowen, R. L., Borchardt, R. T., and Yin, D. H. (2003) *Trypanosoma cruzi*: Molecular cloning and characterization of the S-adenosylhomocysteine hydrolase. *Exp. Parasitol. 105*, 149–158.
3. Creedon, K. A., Rathod, P. K., and Wellems, T. E. (1994) *Plasmodium falciparum* S-adenosylhomocysteine hydrolase. cDNA identification, predicted protein sequence, and expression in *Escherichia coli*. *J. Biol. Chem. 269*, 16364–16370.
4. Yang, X., and Borchardt, R. T. (2000) Overexpression, purification, and characterization of S-adenosylhomocysteine hydrolase from *Leishmania donovani*. *Arch. Biochem. Biophys. 383*, 272–280.
5. Chiang, P. K. (1998) Biological effects of inhibitors of S-adenosylhomocysteine hydrolase. *Pharmacol. Ther. 77*, 115–134.
6. Yang, X., Hu, Y., Yin, D. H., Turner, M. A., Wang, M., Borchardt, R. T., Howell, P. L., Kuczera, K., and Schowen, R. L. (2003) Catalytic strategy of S-adenosyl-L-homocysteine hydrolase: Transition-state stabilization and the avoidance of abortive reactions. *Biochemistry 42*, 1900–1909.
7. Li, Q.-S., Cai, S., Borchardt, R. T., Fang, J., Kuczera, K., Middaugh, C. R., and Schowen, R. L. (2007) Comparative kinetics of cofactor association and dissociation for the human and trypanosomal S-adenosylhomocysteine hydrolases. 1. Basic features of the association and dissociation processes. *Biochemistry 46*, 5798–5809.
8. Teixeira, R. A., Nitz, N., Guimaro, M. C., Gomes, C., and Santos-Buch, C. A. (2006) Chagas disease. *Postgrad. Med. J. 82*, 788–798.
9. Hu, Y., Komoto, J., Huang, Y., Gomi, T., Ogawa, H., Takata, Y., Fujioka, M., and Takusagawa, F. (1999) Crystal structure of S-adenosylhomocysteine hydrolase from rat liver. *Biochemistry 38*, 8323–8333.
10. Kollman, P. A., Massova, I., Reyes, C., Kuhn, B., Huo, S. H., Chong, L., Lee, M., Lee, T., Duan, Y., Wang, W., Donini, O., Cieplak, P., Srinivasan, J., Case, D. A., and Cheatham, T. E. (2000) Calculating structures and free energies of complex molecules: Combining molecular mechanics and continuum models. *Acc. Chem. Res. 33*, 889–897.
11. Jorgensen, W. L., Chandrasekhar, J., Madura, J. D., Impey, R. W., and Klein, M. L. (1983) Comparison of simple potential functions for simulating liquid water. *J. Chem. Phys. 79*, 926–935.
12. Jakalian, A., Bush, B. L., Jack, D. B., and Bayly, C. I. (2000) Fast, efficient generation of high-quality atomic charges. AM1-BCC model: I. Method. *J. Comput. Chem. 21*, 132–146.
13. Sugui, C., and Darden, T. A. (1999) Molecular dynamics simulations of biomolecules: Long-range electrostatic effects. *Annu. Rev. Biophys. Biomol. Struct. 28*, 155–179.
14. Miyamoto, S., and Kollman, P. A. (1992) Settle: An Analytical Version of the Shake and Rattle Algorithm for Rigid Water Models. *J. Comput. Chem. 13*, 952–962.
15. Gohlke, H., Kiel, C., and Case, D. A. (2003) Insights into protein-protein binding by binding free energy calculation and free energy decomposition for the Ras-Raf and Ras-RaIGDS complexes. *J. Mol. Biol. 330*, 891–913.
16. Cai, S., Li, Q. S., Borchardt, R. T., Kuczera, K., and Schowen, R. L. (2007) The antiviral drug ribavirin is a selective inhibitor of S-adenosyl-L-homocysteine hydrolase from *Trypanosoma cruzi*. *Bioorg. Med. Chem. 15*, 7281–7287.
17. Li, Q.-S., Cai, S., Fang, J., Borchardt, R. T., Kuczera, K., Middaugh, C. R., and Schowen, R. L. (2008) Comparative kinetics of cofactor association and dissociation for the human and trypanosomal S-adenosylhomocysteine hydrolases. 2. The role of helix 18 stability. *Biochemistry 47*, 4983–4991.
18. Turner, M. A., Yuan, C. S., Borchardt, R. T., Hershfield, M. S., Smith, G. D., and Howell, P. L. (1998) Structure determination of selenomethionyl S-adenosylhomocysteine hydrolase using data at a single wavelength. *Nat. Struct. Biol. 5*, 369–376.
19. Ault-Riche, D. B., Yuan, C. S., and Borchardt, R. T. (1994) A single mutation at lysine 426 of human placental S-adenosylhomocysteine hydrolase inactivates the enzyme. *J. Biol. Chem. 269*, 31472–31478.